ACS APPLIED MATERIALS & INTERFACES

www.acsami.org

Research Article

Complex Phase Transitions of Fully Rigid Sphere–Rod Amphiphiles Induced by Solvent Polarity in Dilute Solutions

Yifan Zhou, Jingfan Wei, Xiangqian Li, Patryk Wąsik, Hao Liu,* and Tianbo Liu*

Cite This: *ACS Appl. Mater. Interfaces* 2024, 16, 51512–51520

Read Online

ACCESS | Metrics & More | Article Recommendations | Supporting Information

ABSTRACT: We report complex macrophase and microphase transitions of rigid amphiphiles with spherical Keggin molecular clusters as the solvophilic block and rod-like rigid oligofluorene (OF) as the solvophobic block in mixed solvents of water and polar organic solvent. By properly adjusting the solvent polarity, the amphiphiles are found to respond accordingly by self-assembling into multilayered incomplete onion-like structures (10–25 vol % THF), single-layered vesicular structures (60 vol % THF), and an unexpected macrophase separation in the middle (40–50 vol % THF), which is due to the anomalous trends in Keggin solubility as a result of the nature of TBA^+ counterions. The rigidity of the OF block prevents the amphiphile from assembling by following the rule of packing parameters; instead, interdigitation among different rods leads to the formation of the solvophobic domain to achieve self-assembly. The incomplete onion structures are controlled by the interdigitation of rigid rods for the number of layers and the electrostatic interaction among Keggin head groups for the interlayer distance. When the degree of interdigitation becomes lower, the self-assembly process shows a trend that can be explained by the traditional rule of packing parameter. This study demonstrates the formation of different self-assembled structures by rigid amphiphiles and their transitions induced by solvent composition. The self-assembly (microphase separation) of rigid amphiphiles in a dilute solution could indeed represent a broad area containing complicated, uncharted rules.

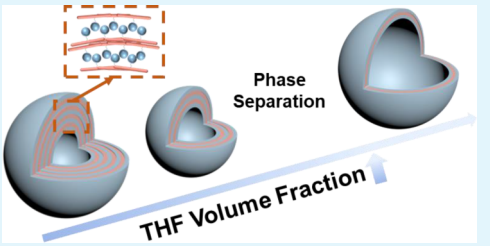

KEYWORDS: *rigid sphere–rod amphiphiles, incomplete onion structure, vesicle, macrophase separation, microphase separation*

Downloaded via UNIV OF AKRON on July 29, 2025 at 18:46:39 (UTC).
See https://pubs.acs.org/sharingguidelines for options on how to legitimately share published articles.

INTRODUCTION

The self-assembly of amphiphiles, such as surfactants[1,2] and block copolymers,[3] in selective solvents has been well explored. Such self-assembly processes are usually driven by the solvophobic interaction, sometimes other noncovalent interactions might also contribute,[4] such as electrostatic interaction, cation-π interaction, hydrogen bonding, and $\pi-\pi$ stacking. It is well accepted that the inherent flexibility of amphiphiles plays a pivotal role in predicting potential structures, mainly based on the packing parameter p[5], with

$$p = v/a_0 l_c \quad (1)$$

where v and l_c represent the volume and length of the hydrophobic blocks, respectively, and a_0 is the contact area of the hydrophilic block. Different packing parameters lead to a sequence of assembled structures: spherical micelles, worm-like micelles, vesicles, bilayers, and their reversed structures when the hydrophobic block becomes more dominant.

A question would naturally be raised: what happens when the blocks in amphiphiles become rigid? Bulky polar head groups, from nanoscale, well-defined inorganic molecular clusters such as polyoxometalates (POMs)[6−10] polyhedral oligomeric silsesquioxane (POSS),[11−15] and fullerenes (C_{60}),[16,17] to organic clusters, such as cyclodextrin (CD)[18,19] and biomolecules[20,21] (e.g., ubiquitin protein), have been used to replace the common small polar head groups of surfactants.[22] These giant surfactants with rigid head groups, in general, still assemble by following the rule of the packing parameter, since the surfactant chain collapse (and the consequent microphase separation) dominantly occurs with the solvophobic domain. On the other hand, for the amphiphiles containing rigid solvophobic blocks (e.g., rod–coil copolymers with rigid rods and flexible coils[23−25]), their assembly behaviors are very different because those rigid solvophobic blocks cannot undergo conformational changes like flexible chains. The situation is expected to be more sophisticated if both solvophilic and solvophobic blocks become bulky and fully rigid. Such solvophobic domains must come together to minimize the free energy but must do so in different ways, making the common rule of the packing parameter for flexible amphiphiles inapplicable. Therefore, exploring the behavior of rigid amphiphiles poses an intriguing but also challenging and poorly charted area.

Fully rigid sphere–rod–sphere amphiphiles with dumbbell-shaped geometry were reported to form different assembly

Received: June 25, 2024
Revised: August 31, 2024
Accepted: September 3, 2024
Published: September 13, 2024

ACS Publications

© 2024 American Chemical Society

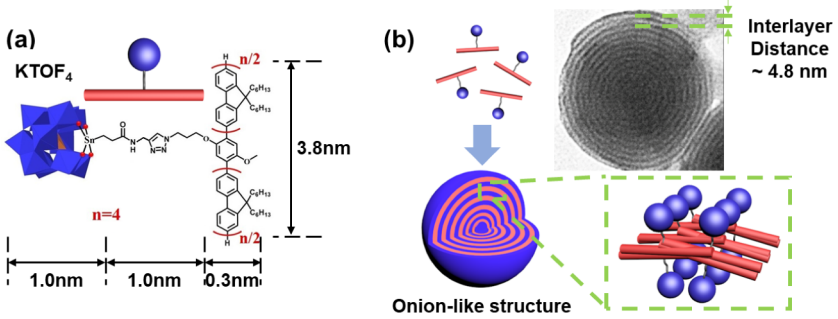

Figure 1. (a) The chemical structure and the model of KTOF4; (b) KTOF4 self-assembles into onion-like structures with an identical interlayer distance by the interdigitation among rods.

structures (vesicles, onion-like, or blackberry-type structures) depending on the driving force of the assembly, the solvent conditions, and/or the length/feature of the rods.[26] The next exciting question is how do the amphiphiles assemble when both blocks being rigid and with comparable volumes, while the solvophobic block being very anisotropic (e.g., rod-like) so that the size, shape, and orientation of the rigid block will all play roles in the packing of this block in its poor solvent.[27−32] Our previous work reported the self-assembly of rigid sphere−rod amphiphilic hybrid macromolecules, which contain the hydrophilic, 1 nm-sized spherical Keggin cluster with four tetrabutyl ammonium (TBA^+) ions as counterions (formula $TBA_4(PW_{11}O_{39})$), chemically linked with an oligofluorene with four repeat units to form a T-shaped amphiphile (named KTOF4) (Figure 1a). Such rigid hybrid amphiphiles could form highly uniform, onion-like supramolecular structures, which are also observed to be formed by other flexible amphiphiles[33,34], in water/acetonitrile mixed solvents.[31] Instead of the variable layer distance and limited layers observed in the onion-like structures formed by the flexible amphiphiles, the onion structures strictly possess an identical interlayer distance of 4.8 nm; and the number of layers (i.e., assembly size) increases with the increasing acetonitrile content or decreasing temperature (i.e., a better solvent for the hybrids) (Figure 1b). We proposed a model to explain this unique self-assembly process, in which two rigid rods first stay close to each other to minimize the free energy, and then such units would interdigitate with each other significantly to form a condensed hydrophobic shell. The interdigitation angle has to be changed for different layers in order to form the onion-like vesicles. Interestingly, as the length of rigid rods increases from 4 (KTOF4, a rod length of ∼3.8 nm) to 6 (KTOF6, a rod length of ∼5.6 nm) repeat units, full onion-like structures become incomplete by losing a few inner layers, which can be explained as longer rods cannot interdigitate into larger curvatures (i.e., smaller shells). The change of assembly sizes is reversible when the solvent content or temperature changes.

It is apparent that the solvent plays a critical and complicated role in the self-assembly of rigid sphere-−rod amphiphiles. A common approach for exploring the solvent effect is to tune the composition of water/organic mixed solvents, leading to a continuous change in solvent polarity.[35,36] The amphiphiles might exist as soluble single molecules or self-assemble into normal/inverse supramolecular structures or experience macrophase separation, depending on the compatibility of different domains in those solvents. The situation for the current hybrid molecules becomes more complicated because they contain multiple domains (a hydrophilic Keggin, a short organic linker, a hydrophobic rigid rod, and short alkyl chains on the rods) as well as additional factors such as charges on the Keggin and the counterions. The influence of the solution condition on the self-assembly of such hybrids is very complicated, and the assembly properties might not always change monotonically with the solvent polarity. Therefore, a systematic study on the solvent effects, including the correlation between the self-assembly behaviors and Hansen solubility parameters,[37] Hildebrand solubility parameters,[38] and modified separation of cohesive energy density (MOSCED),[39] becomes necessary.

In this work, we will focus on exploring the effects of solvent composition on the self-assembly of sphere−rod rigid amphiphiles, including the corresponding changes in the assembled structures and their other features, to understand the mechanism of this new type of self-assembly favored by rigid amphiphiles. KTOF6 is selected as the rigid amphiphile here. Considering a significant difference in dielectric constants (tetrahydrofuran (THF) ∼ 7.58[40] and water ∼ 80.1[41] at 20 °C), THF/water mixed solvents are used to achieve a broad range of solvent polarity. Consequently, two other water-miscible organic-solvent-based solvent systems (dioxane/water and acetone/water) are used to further explore the versatility of the KTOF6 solution behaviors.

RESULTS AND DISCUSSION

Synthesis of Keggin T-Shape-Linked Oligofluorene Giant Surfactant Amphiphilic Hybrids. The synthesis of KTOF6 amphiphilic hybrids followed a previously established method[31] (Figure S1). Specifically, KTOF6 is designed as a T-shaped sphere−rod complex macromolecule by conjugating (i) alkyne-functionalized Keggin-type polyoxotungstate $TBA_4(PW_{11}O_{39})(SnCH_2CH_2CONHCH_2CCH)$ as the solvophilic polar headgroup, which was synthesized based on the procedure in the Supporting Information, with (ii) an azide-functionalized rigid oligofluorene (OF) rod comprising six repeating units as the solvophobic domain, via the copper-catalyzed azide−alkyne cycloaddition (CuAAC) reaction (Figure 2). The main products of Br-TOF6, N3-TOF6, and KTOF6 obtained in this process have been conclusively confirmed by ^1H NMR (Figures S2−S4).

Solubility of KTOF6 in Mixed Solvents. Considering that KTOF6 contains a hydrophilic Keggin-type cluster and a rigid hydrophobic OF rod, it is expected to be amphiphilic in both polar and nonpolar solvents. To this end, THF and water were selected as nonpolar and polar solvents, respectively, mainly due to their good miscibility and the substantial disparity in their dielectric constants (i.e., THF ∼ 7.58 and

https://doi.org/10.1021/acsami.4c10543
ACS Appl. Mater. Interfaces 2024, 16, 51512−51520

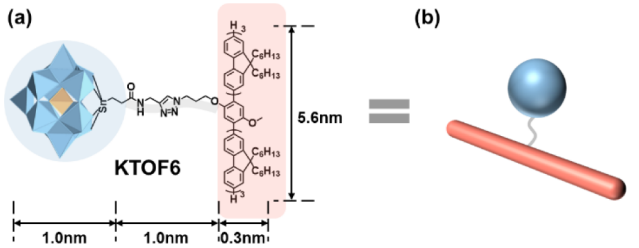

Figure 2. (a) Keggin T-shape-linked oligofluorene (KTOF6), counterion TBA^+ is omitted for clarity; (b) sphere−rod model.

water ~80.1 at 20 °C). For the whole macromolecule, THF is a good solvent (especially for the OF rod, Figure S16b), while water acts as a poor solvent but is more compatible with the Keggin clusters. To investigate the self-assembly behaviors of KTOF6 in solvents with various polarities, THF and water mixed solvents with different THF volume fractions (i.e., 0−100 vol %) are applied, and a concentration of 0.1 mg/mL was set. 0.1 mg/mL of KTOF6 is soluble when the THF volume fraction is 10−30% and 60−90%, while KTOF6 precipitates out in the 40−50 vol % THF and water mixed solvent.

Self-Assembly of KTOF6 into Incomplete Onion-Like Structures in THF/Water Mixed Solvents with a Dominant Amount of Water. Static light scattering (SLS) was first employed to confirm the formation of self-assembled structures by KTOF6, as indicated by a drastic jump in the scattered intensity. Specifically, the scattered intensity of KTOF6 dissolved in pure THF is relatively low, indicating that KTOF6 exists as single molecules in the THF solvent. That is, THF is a good solvent for KTOF6. Such low scattered intensity of KTOF6 is also observed when the volume fraction of THF is 70−90 vol %, indicating that KTOF6 behaves in the manner of single molecules in these solvents. In contrast, KTOF6 tended to self-assemble in the THF/water mixed solvent with THF content at 10−25 and 60 vol %, leading to high scattered intensity in SLS, a typical indicator of large assemblies.

Dynamic light scattering (DLS) was further used to confirm the hydrodynamic size/size distribution of self-assembled KTOF6. For samples in mixed solvents containing THF between 10 and 25 vol %, the CONTIN analysis[42] from the DLS measurements at a scattering angle of 90° showed large supramolecular structures with narrow size distributions. A decrease in the hydrodynamic radius (R_h) of the assemblies was observed from ~48.4 to ~34.3 nm as the THF volume fraction increased from 10 to 25 vol % (Figure 3a). In 10% THF solution, the R_h values of KTOF6 assemblies show no dependence on the scattering angle (Figure S5a), illustrating their isotropic nature. This is further confirmed by transmission electron microscopy (TEM) studies (Figure 3c), where the spherical morphology can be clearly observed. Furthermore, the ratio of R_g (~46.2 nm from SLS in Figure S5b) and R_h (~48.4 nm from DLS) is 0.95, which lies between the values of a solid sphere (0.77) and a single-layer hollow sphere (1.00), but closer to 1, thus strongly suggesting the presence of multilayer vesicular structures with a hollow center.[43] Evidently, the TEM images in Figure 3c clearly

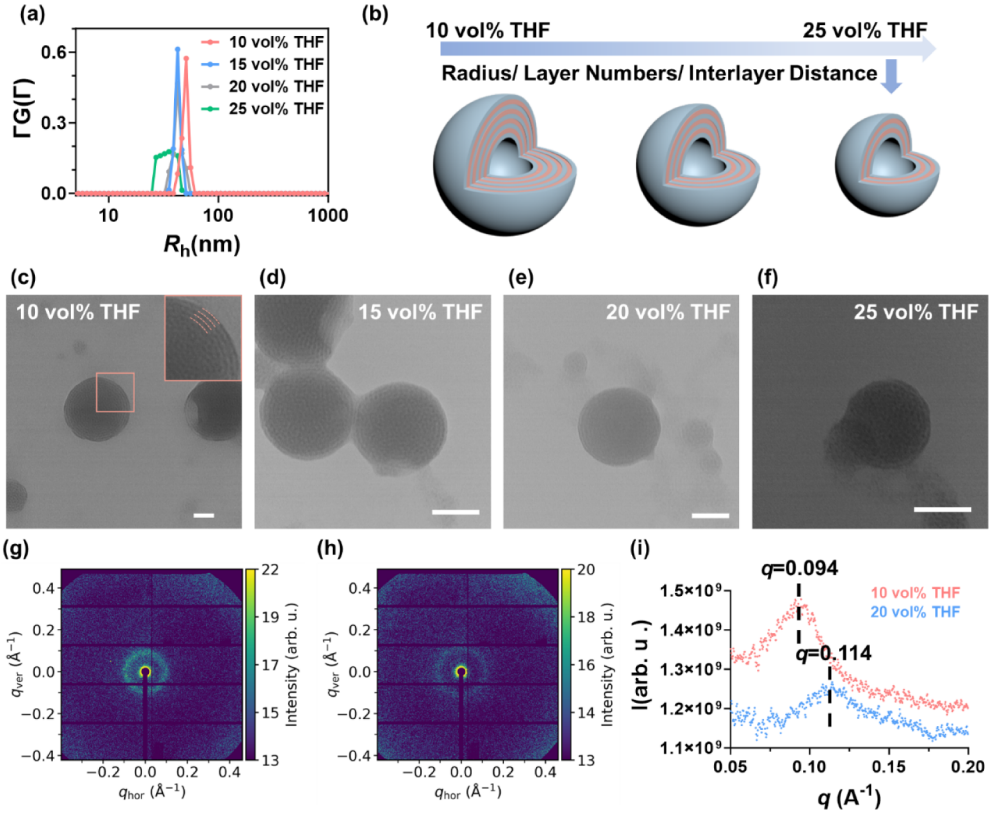

Figure 3. (a) CONTIN analysis of KTOF6 in 10−25 vol % THF and water mixed solvents; (b) schematic illustration of the evolution of incomplete onion structures from 10 vol % to 25 vol % THF; TEM images (scale bar: 50 nm) of KTOF6 (0.1 mg/mL) in (c) 10 vol % THF, (d) 15 vol % THF, (e) 20 vol % THF, (f) 25 vol % THF; SAXS patterns of KTOF6 (0.1 mg/mL) in (g) 10 vol % THF, (h) 20 vol % THF; (i) I vs q SAXS plot corresponding the KTOF6 (0.1 mg/mL) in 10 vol % THF and 20 vol % THF.

https://doi.org/10.1021/acsami.4c10543
ACS Appl. Mater. Interfaces 2024, 16, 51512−51520

showed incomplete onion structures, i.e., hollow spherical structures with outer layers rather than complete onion-like KTOF4 assemblies. Quantitively, KTOF6 assemblies displayed hollow spherical structures consisting of more than 3 layers with an average radius of ~43 nm (consistent with the R_h value in DLS), and a consistent, well-defined interlayer distance of ~5.5 nm (Figures 3c and S6).

Small-angle X-ray scattering (SAXS) study on KTOF6 in the water/THF mixed solvent with 10% THF reveals a dominant diffraction peak (Figure 3g) at $q \sim 0.094$ Å^{-1}, which corresponds to an ordered packing of ~6.7 nm (Figure 3i). This distance is very likely to be the interlayer distance within the incomplete onion-like structures. The interlayer distance observed in TEM is smaller than that in SAXS, mainly due to the loss of solvent molecules during the drying process of the TEM grids.

Meanwhile, with the increasing THF volume fraction to 15%, 20%, and 25%, the KTOF6 assemblies become smaller, containing fewer layers with closer interlayer distances (Table 1). SAXS data show that the interlayer distance calculated for the assemblies in 20 vol % THF is ~5.5 nm (q of ~0.114 Å^{-1}, Figure 3i), confirming a decrease when the THF volume fraction increases from 10% to 20%, matching the observation of interlayer distance in TEM. Collectively, KTOF6 formed incomplete onion-like structures in 10−25 vol % THF solvents, with decreasierlayer distances in higher THF content solutions (Figure 3b).

Table 1. Size, Number of Layers, and Interlayer Distances of KTOF6 Assemblies in 10−25 vol % THF, Summarized from Figures S5−S10 and 3a,3c−f

THF vol %	10%	15%	20%	25%
R_h (nm)	~48.4	~43.4	~42.7	~34.3
radius in TEM (nm)	~43	~40	~39	~31
number of layers	>3 layers	2−3 layers	1−2 layers	1 layer with some incomplete layers
interlayer distance in TEM (nm)	~5.5	~5.2	~5.1	N/A

The solvent conditions evidently play a crucial role in the structural evolution of the KTOF6 assemblies. At the core of this phenomenon, an inverse relationship lies between the volume fraction of tetrahydrofuran (THF) and the strength of the hydrophobic interaction: as the THF volume fraction increases, solvent polarity decreases, consequently diminishing the strength of hydrophobic interactions. In essence, the reduced requirement for the close packing of hydrophobic domains in less polar solvents not only results in less significant interdigitation among the rigid OF rods but also facilitates greater flexibility in the hydrophobic layer, leading to a reduction in the assembly size attributed to the formation of larger curvatures.

Moreover, our previous findings indicate that the formation of multilayer structures by such rigid sphere−rod amphiphiles is predominantly driven by significant interdigitation among the rigid rods. Herein, when the solvent is less polar, the decrease in layer numbers of the KTOF6 assemblies mainly stems from the less significant interdigitation. Notably, in comparison to the identical interlayer distance of the onion-like structures formed by KTOF4, the interlayer distance can be controlled by the solvent polarity, which is interpreted as being regulated by the electrostatic repulsion among Keggins and will be further explored in the "Mechanism of the Phase Transitions in THF/Water Mixed Solvents" section. Quanti-

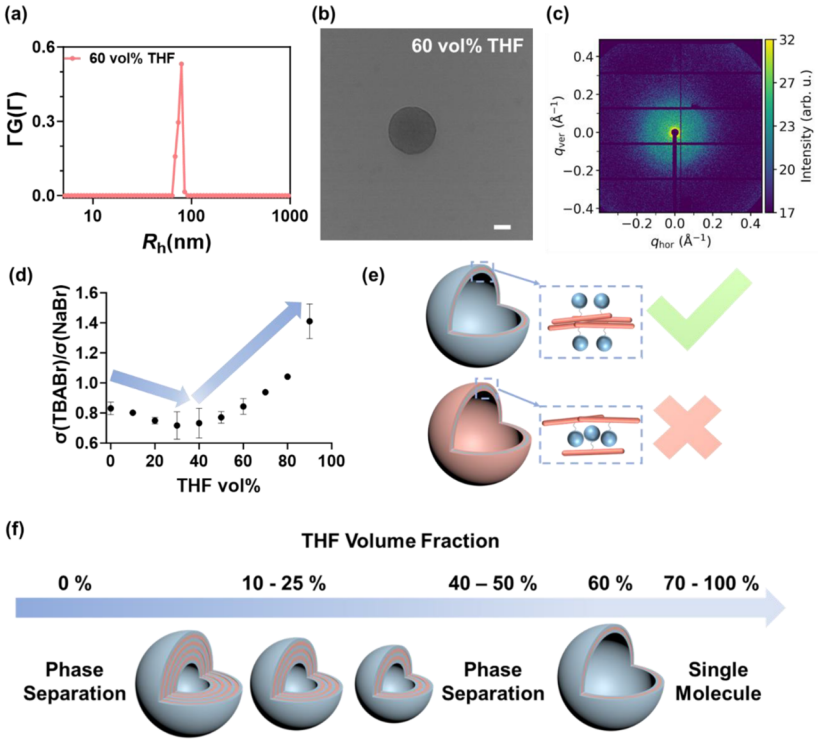

Figure 4. (a) CONTIN analysis, (b) TEM images (scale bar: 50 nm), and (c) SAXS pattern of 0.1 mg/mL of KTOF6 in 60 vol % THF and water mixed solvent; (d) σ(TBABr)/ σ(NaBr) ratios at different THF volume fractions; (e) schematic illustration of the vesicles' formation; (f) schematic illustrations of self-assembly behaviors: 0.1 mg/mL of KTOF6 at different THF volume fractions.

https://doi.org/10.1021/acsami.4c10543
ACS Appl. Mater. Interfaces 2024, 16, 51512−51520

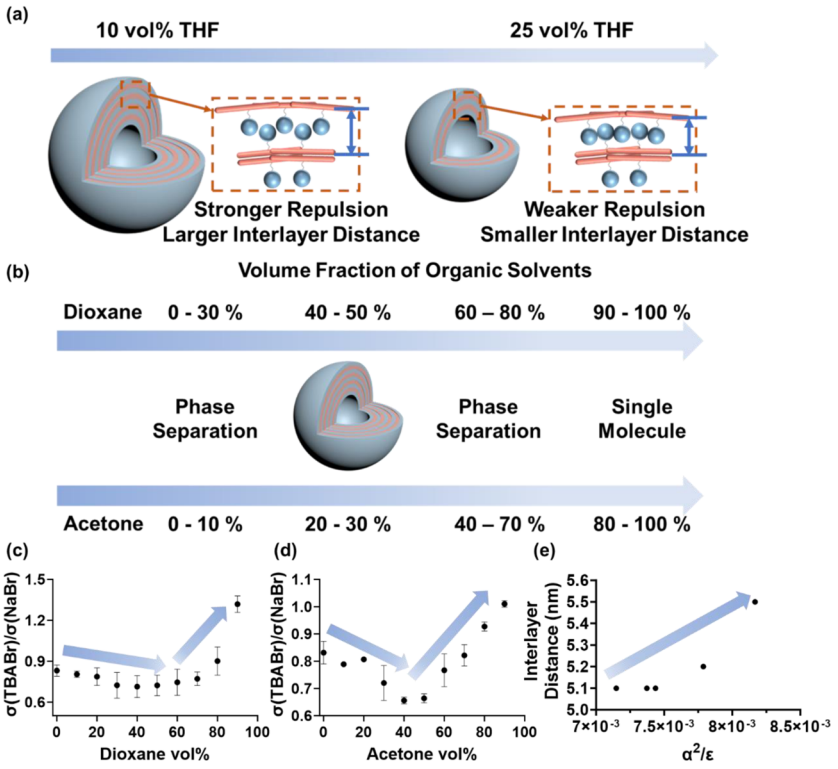

Figure 5. (a) Schematic illustration of the decrease of the interlayer distance when the THF volume fraction increases from 10% to 25%; (b) schematic illustrations of self-assembly behaviors: 0.1 mg/mL of KTOF6 at different dioxane volume fractions and 0.3 mg/mL of KTOF6 at different acetone volume fractions; σ(TBABr)/σ(NaBr) ratios at different (c) dioxane volume fractions and (d) acetone volume fractions; (e) interlayer distance vs α^2/ε.

tively, the interlayer distance of the complete onion formed by KTOF4 is 4.8 nm, which is much smaller than the interlayer distances observed in the incomplete onions, because longer rigid rods lead to the formation of thicker layers inevitably when they interdigitate with each other.

Formation of Single-Layer Vesicular Structures in Less Polar Mixed Solvents. Similarly, in the case of spherical KTOF6 assemblies in THF/water mixed solvents with 60 vol % THF, $R_h \sim 79.1$ nm (Figure 4a) and $R_g \sim 75.6$ nm were obtained from light scattering experiments, indicating an R_g/R_h ratio of 0.96 (Figure S11), suggesting a hollow spherical structure. TEM images show the hollow vesicular structures clearly (Figures 4b and S12). Meanwhile, no peak is observed in its SAXS curve, indicating that there is no multilayer packing in the supramolecular structures (Figure 4c), further confirming the hollow, likely single-layered vesicular structures.

To further investigate whether KTOF6 forms vesicles in less polar solvents, higher concentrations (0.2 mg/mL) of KTOF6 were used to study the self-assembly behavior. In the case of 60 vol % THF, KTOF6 was confirmed to form vesicles, as evidenced by the vesicular structures in TEM and $R_h \sim 104.9$ nm in DLS (Figure S13). Such vesicles can also be formed in a lower solvent polarity by slightly increasing the THF volume fraction from 60% to 65%, which was confirmed by DLS and TEM (Figure S14). Therefore, it is proved to be inevitable that KTOF6 can self-assemble into vesicular structures in less polar solvents instead of it being a coincidence that 0.1 mg/mL of KTOF6 self-assembles into vesicles in 60% THF.

Typically, amphiphiles form the vesicles and reversed vesicles in polar solvents and nonpolar solvents, respectively, with the flexibility to realize mutual transition by tuning the solvent polarity. It is well accepted that such transitions between vesicles and reversed vesicles usually behave as soluble single molecules or precipitation because of the lack of selectivity to both blocks of the amphiphiles. So, the observed precipitation appears to stem from the transition between the vesicle and reversed vesicles. However, solubility tests confirmed that Keggins are the solvophilic blocks of KTOF6 (Figure S16), indicating that the Keggins consistently orient themselves toward the solvent (Figure 4e) during the polarity adjustment process tuned by THF composition, i.e., Keggins did not reach the reversed state where they would be hiding themselves from the solvent.

Abnormal Precipitation Observed in the THF/Water Mixed Solvents with 40−50 Vol % THF. Precipitation observed in the middle range of water/THF mixed solvents (40−50 % THF) is unexpected since KTOF6 is soluble in solvents on both water-rich and THF-rich sides. TEM studies indeed show random aggregates with very large sizes in the TEM (Figure S15), confirming that macrophase separation occurred in solution. In the normal case, as the proportion of the good solvent increases, amphiphiles are expected to become more and more soluble. However, in our study, as the THF (i.e., good solvent) fraction increased, KTOF6 was first soluble, formed precipitates, and then became soluble again in the THF/water mixed solvents.

To understand this phenomenon, it is important to analyze the solubility of each component in the hybrid macromolecule. The straightforward solubility test reveals that Keggins are soluble when the THF volume fraction is from 0% to 60% and cannot be dissolved in pure THF (Figure S16a). The hydrophobic rod block of KTOF6 is insoluble at 10−60 vol

https://doi.org/10.1021/acsami.4c10543
ACS Appl. Mater. Interfaces 2024, 16, 51512−51520

% THF (Figure S16b). Moreover, the Keggin cluster is hydrophilic overall, especially when carrying charges. However, the number of effective charges on the Keggin is difficult to measure accurately due to counterion association, especially in the mixed solvents.

To solve this problem, a new experiment is designed to measure the quantitative counterion dissociation around Keggins by measuring solution conductivity. The conductivity (σ) of both 10 μM sodium bromide (NaBr) and tetrabutylammonium bromide (TBABr) were first measured in a series of THF−water mixed solvents (Figure S17), followed by the calculation of the ratio of σ(TBABr)/σ(NaBr), which indicates the degree of TBA^+ counterion dissociation. Due to the existence of water and the high solubility of NaBr in water, the dissociation of NaBr is assumed as 100%. Hence, the conductivity of NaBr is applied as the denominator for the calibration. Then, the resulting ratio of σ(TBABr)/σ(NaBr) can demonstrate the dissociation of TBABr in the corresponding mixed solvents. As shown in Figure 4d, as the THF vol % increases from 0% to 90%, the dissociation of the counterions was first decreased and then increased, with the lowest point at ∼40%, which is consistent with previously observed abnormal precipitation. Therefore, it is reasonable to conclude that the precipitation is caused by the least solubility of solvophilic POMs and the poor solubility of solvophobic rigid rods. This hypothesis was subsequently validated by SLS, which showed the highest scattered intensity (due to the formation of very large aggregates) of POMs in 40 vol % THF (Figure S18). Overall, this expected macrophase separation is a result of using TBA^+ counterions for the Keggin clusters.

The Mechanism of the Phase Transitions in THF/Water Mixed Solvents. As discussed in the "Self-Assembly of KTOF6 into Incomplete Onion-Like Structures in THF/Water Mixed Solvents with a Dominant Amount of Water" section, in solvents with higher polarity, specifically for the THF/water mixture with 10−25 vol % THF, KTOF6 self-assembles into incomplete onion-like structures (Figure 4f), with their size, layer number, and interlayer distance decreasing with the increasing THF fraction. The reduction in size and layer numbers is predominantly governed by the polarity of the solvent, which in turn impacts: (i) the strength of hydrophobic interactions, (ii) the degree of interdigitation among the rigid rods, and (iii) the flexibility of the hydrophobic layers of assemblies. More specifically, with increasing THF vol % (i.e., lower solvent polarity), the hydrophobic interaction is weakened, leading to less significant interdigitation (i.e., fewer layers) and greater hydrophobic layer flexibility (i.e., larger curvature, aka smaller size). Additionally, the electrostatic interaction between Keggins is believed to play an important role in regulating the interlayer packing, which is feasible to be proven by the self-assembly of the pure OF rods in dilute solution. This is indicated by the absence of layer-by-layer structures and instead vesicular assembly structures with R_h of 103.6 nm (Figures S19 and S20) in pure OF6 rods formed in 10 vol % THF and water mixed solvent. Therefore, the decreased interlayer distance is attributed to the decreased electrostatic repulsion among the Keggins (Figure 5a), as evidenced by the decreased charges of Keggins with the increasing THF vol % from 10% to 25%.

Packing parameters (eq 1), a crucial concept to determine the morphologies of the self-assembled structures, are calculated as 0.79 based on KTOF6 geometry, where v is 0.54 nm^3, a_0 is 1.96 nm^2, and l_c is 0.35 nm, which correspond to the vesicular structures. Theoretically, due to the rigidity of solvophobic blocks, the value of the packing parameter is expected to remain at 0.79 (i.e., vesicular structure) when the THF volume fraction is 10−60%. However, in our study, KTOF6 can only form vesicles in 60 vol % THF, which can be explained by the less significant interdigitation (Figure 4f) to follow the packing parameters.

When the polarity is moderate, KTOF6 precipitates out, which is attributed to the lowest solubility contributed by insoluble OF rod blocks and soluble Keggin clusters with relatively lower solubility, instead of the loss of solvent selectivity to KTOF6 (Figure 4f).

Solution Behaviors of KTOF6 in Other Solvent Systems. The intriguing KTOF6 solution behaviors are not only observed in the THF/water mixed solvent but also found in other solvent systems. Two more water-miscible organic solvents, dioxane and acetone, have been selected as the nonpolar solvents to form the dioxane/water and acetone/water mixed solvent systems. Interestingly, the solution behaviors of KTOF6 in these two mixed solvent systems are similar to the solution behaviors in the THF/water mixed solvent, which is evident in (i) the formation of incomplete onion-like structures in the relatively higher polar solvents (40−50 vol % dioxane and 20−30 vol % acetone) (Figures S21−23), and (ii) the abnormal precipitation when the solvent polarity is adjusted to the intermediate polar (60−80 vol % dioxane and 40−70 vol % acetone), where the Keggins have less charge dissociation, indicating the least solubility of the hydrophilic domains (Figure 5b−d). However, the vesicles are not observed when the solvent polarity is less polar, which is different from the formation of vesicles during the self-assembly of KTOF6 in the THF/water mixed solvents. It is well accepted that the possible reason for this is that the concentration of KTOF6 is unable to approach the critical self-assembly concentration.

It is also reasonable to check if our proposed mechanism works in different solvent systems. Based on our explanation, the interlayer distance is controlled by the electrostatic interaction among the Keggin groups, which is further controlled by the charges on the Keggin head groups. When the interlayer distance in different solvent systems is compared, one could also include the polarity of different solvents. The combined effect of charges and solvent polarity determines the magnitude of electrostatic interactions, which are governed by the dielectric constant and the charges. Herein, the conductivity ratio indicates the charges on the Keggin clusters, and the dielectric constants are measured by the dielectric constant meters (Table S1). Consequently, the electrostatic interaction is proportional to the calculated ratio α^2/ε, that is,

$$F = \frac{1}{4\pi\varepsilon}\frac{qq'}{r^2} \propto \frac{\alpha^2}{\varepsilon} \tag{2}$$

where ε is the dielectric constant and α is the ratio of the conductivity of TBABr and NaBr, i.e.,

$$\alpha = \frac{\sigma(\mathrm{TBABr})}{\sigma(\mathrm{NaBr})} \tag{3}$$

Hence, when α^2/ε becomes larger, the repulsion among Keggin clusters increases, which leads to an increase in the interlayer distance (Figure 5e).

https://doi.org/10.1021/acsami.4c10543
ACS Appl. Mater. Interfaces 2024, 16, 51512−51520

CONCLUSION

The complex solution behaviors of the amphiphilic rigid sphere−rod amphiphiles, including their macrophase and microphase separations in mixed solvents of water and organic solvents, are reported. The self-assembly of incomplete onion-like structures is observed in THF/water mixed solvents containing 10−25 vol % THF. Meanwhile, single-layer vesicular assembly structures, apparently following the rule of packing parameters for flexible amphiphiles, are observed in 60 vol % THF, i.e., much less polar solvents. An unexpected precipitation process (macrophase separation) occurs in the middle (40−50 vol % THF) due to the nature of organic counterions (TBA^+), which affects the solubility of the Keggin clusters via counterion dissociation. Moreover, the evolution of the incomplete onion structures is found to be controlled by both the interdigitation of the rigid rods and electrostatic interactions among Keggins. The interdigitation of rods, influenced by the strength of the hydrophobic interaction (related to the solvent polarity), controls the layer numbers and the size of the overall assemblies, while the delicate balance among the charged Keggins plays a vital role in the interlayer packing and distance.

The common rule of packing parameters for amphiphiles is inapplicable for the current molecules due to their chain rigidity, especially when the degree of interdigitation is significant. However, it is still instructive when the degree of interdigitation is limited. Similar solution behaviors of KTOF6 are also observed in other solvent systems such as dioxane/water and acetone/water mixed solvents. Overall, the rigid amphiphile KTOF6 and the previously reported KTOF4 demonstrate the complex and fascinating self-assembly behaviors of rigid amphiphiles, which are different from flexible amphiphiles and still poorly understood, but obviously with some clear trends for more systematic future explorations.

MATERIALS AND METHODS

Materials. All of the chemicals related to the synthesis, including raw materials, catalysts, and other agents, were purchased from Sigma, Oakwood, or Fisher. The solvents for solution preparation are 1,4-dioxane (Sigma, 99.8%), tetrahydrofuran (Sigma, 99.9%), and acetone (Fisher, certified ACS). Water was purified by a Milli-Q DirectQ3 water purification system. PTFE syringe filters were purchased from Millipore.

Sample Preparation. The KTOF6 samples were dissolved in anhydrous THF. The stock solutions at a concentration of 1.0 mg/mL were filtered using a hydrophilic PTFE syringe filter with a 0.22 μm pore size. Then, the stock solutions were diluted by adding extra filtered THF solvent. The solvent ratio was adjusted by slowly adding filtered Milli-Q water dropwise under stirring.

Dynamic Light Scattering (DLS) and Static Light Scattering (SLS). A Brookhaven Instruments light scattering spectrometer equipped with a diode-pumped solid-state (DPSS) laser operating at 532 nm and a BI-9000AT multichannel digital correlator were applied to perform DLS and SLS measurements. SLS was operated based on the Rayleigh−Gans−Debye equation. The radius of gyration (R_g) was obtained from a partial Zimm plot following an approximate equation: $1/I = C\ (1 + R_g^2 q^2/3)$, where the momentum transfer q equals $4\pi/\lambda\ \sin(\theta/2)$. For DLS, the constrained regularized (CONTIN) method was used to convert the intensity−intensity time correlation functions. The average apparent translational diffusion coefficient, D_{app}, was determined from the normalized distribution function of the characteristic line width, $\Gamma(G)$. The particle size distribution in the solution can be obtained from a plot of $\Gamma G(\Gamma)$ versus the average hydrodynamic radius (R_h). R_h was converted from D through the Stokes−Einstein equation: $R_h = KT/6\pi\eta D$, where K is the Boltzmann constant and η is the solvent's viscosity at temperature T.

Nuclear Magnetic Resonance (NMR). ^{1}H NMR spectra were measured on a Varian NMRS 500 spectrometer equipped with a 5 mm dual-broad-band probe. Baseline, phase correction, and data analysis were performed using the MestReNova software.

Transmission Electron Microscopy (TEM). TEM bright-field images were taken on a JEOL JEM-1230 electron microscope operated at 100/110 kV. TEM samples were prepared by dropping ~4 μL solution samples on carbon-film-covered copper grids and drying under vacuum at room temperature. The radius, number of layers, and interlayer distance of multiple spheres were calculated through ImageJ software.

Small-Angle X-Ray Scattering (SAXS). Synchrotron SAXS measurements were performed at the 12-ID (SMI) beamline at NSLS-II, Brookhaven National Laboratory. To carry out the SAXS measurement, a KTOF6 solution was loaded in quartz capillary tubes of 1.5 mm diameter. The measurement was done with X-ray of energy of 16.10 keV with a sample-to-detector distance of 1.6 m. A Pilatus3 1 M detector was used for obtaining the SAXS pattern of the sample. The momentum transfer, q, value can be used to calculate the interlayer distance, d, using the equation

$$d = 2 \times \pi/q \tag{4}$$

ASSOCIATED CONTENT

Supporting Information

The Supporting Information is available free of charge at https://pubs.acs.org/doi/10.1021/acsami.4c10543.

Synthetic procedures; NMR characterizations of final products; SAXS, DLS, SLS, and TEM results (PDF)

AUTHOR INFORMATION

Corresponding Authors

Hao Liu − *State Key Laboratory for Modification of Chemical Fibers and Polymer Materials, Center for Advanced Low-Dimension Materials, Donghua University, Shanghai 201620, China;* orcid.org/0000-0002-8390-2696; Email: liuh@dhu.edu.cn

Tianbo Liu − *School of Polymer Science and Polymer Engineering, The University of Akron, Akron, Ohio 44325, United States;* orcid.org/0000-0002-8181-1790; Email: tliu@uakron.edu

Authors

Yifan Zhou − *School of Polymer Science and Polymer Engineering, The University of Akron, Akron, Ohio 44325, United States;* orcid.org/0000-0002-8361-2189

Jingfan Wei − *School of Polymer Science and Polymer Engineering, The University of Akron, Akron, Ohio 44325, United States*

Xiangqian Li − *State Key Laboratory for Modification of Chemical Fibers and Polymer Materials, Center for Advanced*

Low-Dimension Materials, Donghua University, Shanghai 201620, China

Patryk Wąsik − *National Synchrotron Light Source II, Brookhaven National Laboratory, Upton, New York 11973, United States;* orcid.org/0000-0002-7447-7472

Complete contact information is available at: https://pubs.acs.org/10.1021/acsami.4c10543

Notes

The authors declare no competing financial interest.

■ ACKNOWLEDGMENTS

T.L acknowledges support from NSF DMR2215190 and the University of Akron. This research used the 12-ID Soft Matter Interfaces beamline of the National Synchrotron Light Source II, a U.S. Department of Energy (DOE) Office of Science User Facility operated for the DOE Office of Science by Brookhaven National Laboratory under Contract No. DE-SC0012704.

■ REFERENCES

(1) Kronberg, B.; Holmberg, K.; Lindman, B. Surfactant Self-Assembly. In *Surface Chemistry of Surfactants and Polymers*. Springer, 2014. 113136

(2) Fong, C.; Le, T.; Drummond, C. J. Lyotropic liquid crystal engineering−ordered nanostructured small molecule amphiphile self-assembly materials by design. *Chem. Soc. Rev.* **2012**, *41* (3), 1297−1322.

(3) Mai, Y.; Eisenberg, A. Self-assembly of block copolymers. *Chem. Soc. Rev.* **2012**, *41* (18), 5969−5985.

(4) Luo, J.; Liu, T. Competition and Cooperation among Different Attractive Forces in Solutions of Inorganic−Organic Hybrids Containing Macroionic Clusters. *Langmuir* **2019**, *35* (24), 7603−7616.

(5) Li, C.; Li, Q.; Kaneti, Y. V.; Hou, D.; Yamauchi, Y.; Mai, Y. Self-assembly of block copolymers towards mesoporous materials for energy storage and conversion systems. *Chem. Soc. Rev.* **2020**, *49* (14), 4681−4736.

(6) Yin, P.; Wu, P.; Xiao, Z.; Li, D.; Bitterlich, E.; Zhang, J.; Cheng, P.; Vezenov, D. V.; Liu, T.; Wei, Y. A Double-Tailed Fluorescent Surfactant with a Hexavanadate Cluster as the Head Group. *Angew. Chem., Int. Ed.* **2011**, *50* (11), 2521−2525.

(7) Zhang, J.; Song, Y.-F.; Cronin, L.; Liu, T. Self-Assembly of Organic−Inorganic Hybrid Amphiphilic Surfactants with Large Polyoxometalates as Polar Head Groups. *J. Am. Chem. Soc.* **2008**, *130* (44), 14408−14409.

(8) Zhang, J.; Song, Y.-F.; Cronin, L.; Liu, T. Reverse-Vesicle Formation of Organic−Inorganic Polyoxometalate-Containing Hybrid Surfactants with Tunable Sizes. *Chem. - Eur. J.* **2010**, *16* (37), 11320−11324.

(9) Yin, P.; Pradeep, C. P.; Zhang, B.; Li, F.-Y.; Lydon, C.; Rosnes, M. H.; Li, D.; Bitterlich, E.; Xu, L.; Cronin, L.; et al. Controllable Self-Assembly of Organic−Inorganic Amphiphiles Containing Dawson Polyoxometalate Clusters. *Chem. - Eur. J.* **2012**, *18* (26), 8157−8162.

(10) Santoni, M.-P.; Pal, A. K.; Hanan, G. S.; Tang, M.-C.; Venne, K.; Furtos, A.; Ménard-Tremblay, P.; Malveau, C.; Hasenknopf, B. Coordination-driven self-assembly of polyoxometalates into discrete supramolecular triangles. *Chem. Commun.* **2012**, *48* (2), 200−202.

(11) Wang, X.-M.; Shao, Y.; Xu, J.; Jin, X.; Shen, R.-H.; Jin, P.-F.; Shen, D.-W.; Wang, J.; Li, W.; He, J.; Ni, P.; Zhang, W.-B. Precision Synthesis and Distinct Assembly of Double-Chain Giant Surfactant Regioisomers. *Macromolecules* **2017**, *50* (10), 3943−3953.

(12) Yu, X.; Yue, K.; Hsieh, I.-F.; Li, Y.; Dong, X.-H.; Liu, C.; Xin, Y.; Wang, H.-F.; Shi, A.-C.; Newkome, G. R.; Ho, R.-M.; Chen, E.-Q.; Zhang, W.-B.; Cheng, S. Z. D. Giant surfactants provide a versatile platform for sub-10-nm nanostructure engineering. *Proc. Natl. Acad. Sci. U. S. A.* **2013**, *110* (25), 10078−10083.

(13) Yu, X.; Zhong, S.; Li, X.; Tu, Y.; Yang, S.; Van Horn, R. M.; Ni, C.; Pochan, D. J.; Quirk, R. P.; Wesdemiotis, C.; Zhang, W.-B.; Cheng, S. Z. D. A Giant Surfactant of Polystyrene−(Carboxylic Acid-Functionalized Polyhedral Oligomeric Silsesquioxane) Amphiphile with Highly Stretched Polystyrene Tails in Micellar Assemblies. *J. Am. Chem. Soc.* **2010**, *132* (47), 16741−16744.

(14) Su, H.; Zheng, J.; Wang, Z.; Lin, F.; Feng, X.; Dong, X.-H.; Becker, M. L.; Cheng, S. Z. D.; Zhang, W.-B.; Li, Y. Sequential Triple "Click" Approach toward Polyhedral Oligomeric Silsesquioxane-Based Multiheaded and Multitailed Giant Surfactants. *ACS Macro Lett.* **2013**, *2* (8), 645−650.

(15) Guo, Q.-Y.; Yan, X.-Y.; Zhang, W.; Li, X.-H.; Xu, Y.; Dai, S.; Liu, Y.; Zhang, B.-X.; Feng, X.; Yin, J.; Han, D.; Huang, J.; Su, Z.; Liu, T.; Huang, M.; Hsu, C.-H.; Cheng, S. Z. D. Ordered Mesoporous Silica Pyrolyzed from Single-Source Self-Assembled Organic−Inorganic Giant Surfactants. *J. Am. Chem. Soc.* **2021**, *143* (33), 12935−12942.

(16) Yu, X.; Zhang, W.-B.; Yue, K.; Li, X.; Liu, H.; Xin, Y.; Wang, C.-L.; Wesdemiotis, C.; Cheng, S. Z. D. Giant Molecular Shape Amphiphiles Based on Polystyrene−Hydrophilic [60]Fullerene Conjugates: Click Synthesis, Solution Self-Assembly, and Phase Behavior. *J. Am. Chem. Soc.* **2012**, *134* (18), 7780−7787.

(17) Modugno, G.; Syrgiannis, Z.; Bonasera, A.; Carraro, M.; Giancane, G.; Valli, L.; Bonchio, M.; Prato, M. The supramolecular design of low-dimensional carbon nano-hybrids encoding a polyoxometalate-bis-pyrene tweezer. *Chem. Commun.* **2014**, *50* (38), 4881−4883.

(18) Zhou, J.; Yin, P.; Gao, Y.; Hu, L.; Liu, T. Spontaneous Self-Assembly of γ-Cyclodextrins in Dilute Solutions with Tunable Sizes and Thermodynamic Stability. *Chem. - Eur. J.* **2015**, *21* (26), 9563−9568.

(19) Chen, J.; Luo, J.; Bekele, S.; Tsige, M.; Liu, T. Rational Control of Self-Recognition of Macroionic γ-Cyclodextrin by Host-Guest Interaction with Super-Chaotropic Borate Cluster Ions. *ChemPluschem* **2020**, *85* (10), 2316−2319.

(20) Su, Z.; Zhang, R.; Yan, X.-Y.; Guo, Q.-Y.; Huang, J.; Shan, W.; Liu, Y.; Liu, T.; Huang, M.; Cheng, S. Z. D. The role of architectural engineering in macromolecular self-assemblies via non-covalent interactions: A molecular LEGO approach. *Prog. Polym. Sci.* **2020**, *103*, 101230.

(21) Yeates, T. O. Geometric Principles for Designing Highly Symmetric Self-Assembling Protein Nanomaterials. *Annu. Rev. Biophys.* **2017**, *46*, 23−42.

(22) Luo, J.; Sun, X.; Yin, J.-F.; Yin, P.; Liu, T. Supramolecular Nanostructures Constructed from Cluster-based Hybrid Macromolecules. *Giant* **2020**, *2*, 100013.

(23) Olsen, B. D.; Segalman, R. A. Self-assembly of rod−coil block copolymers. *Mater. Sci. Eng., R* **2008**, *62* (2), 37−66.

(24) Xu, L.; Zhou, L.; Li, Y.-X.; Gao, R.-T.; Chen, Z.; Liu, N.; Wu, Z.-Q. Thermo-responsive chiral micelles as recyclable organocatalyst for asymmetric Rauhut-Currier reaction in water. *Nat. Commun.* **2023**, *14* (1), 7287.

(25) Liu, N.; Gao, R.-T.; Wu, Z.-Q. Helix-Induced Asymmetric Self-Assembly of π-Conjugated Block Copolymers: From Controlled Syntheses to Distinct Properties. *Acc. Chem. Res.* **2023**, *56* (21), 2954−2967.

(26) Liu, H.; Luo, J.; Shan, W.; Guo, D.; Wang, J.; Hsu, C.-H.; Huang, M.; Zhang, W.; Lotz, B.; Zhang, W.-B.; Liu, T.; Yue, K.; Cheng, S. Z. D. Manipulation of Self-Assembled Nanostructure Dimensions in Molecular Janus Particles. *ACS Nano* **2016**, *10* (7), 6585−6596.

(27) Zhang, R.; Su, Z.; Yan, X.-Y.; Huang, J.; Shan, W.; Dong, X.-H.; Feng, X.; Lin, Z.; Cheng, S. Z. D. Discovery of Structural Complexity through Self-Assembly of Molecules Containing Rodlike Components. *Chem. - Eur. J.* **2020**, *26* (30), 6741−6756.

(28) Lin, Z.; Yang, X.; Xu, H.; Sakurai, T.; Matsuda, W.; Seki, S.; Zhou, Y.; Sun, J.; Wu, K.-Y.; Yan, X.-Y.; Zhang, R.; Huang, M.; Mao, J.; Wesdemiotis, C.; Aida, T.; Zhang, W.; Cheng, S. Z. D.

Topologically Directed Assemblies of Semiconducting Sphere−Rod Conjugates. *J. Am. Chem. Soc.* **2017**, *139* (51), 18616−18622.
(29) Zhang, R.; Feng, X.; Zhang, R.; Shan, W.; Su, Z.; Mao, J.; Wesdemiotis, C.; Huang, J.; Yan, X.-Y.; Liu, T.; Li, T.; Huang, M.; Lin, Z.; Shi, A.-C.; Cheng, S. Z. D. Breaking Parallel Orientation of Rods via a Dendritic Architecture toward Diverse Supramolecular Structures. *Angew. Chem., Int. Ed.* **2019**, *58* (34), 11879−11885.
(30) Yan, X.-Y.; Lin, Z.; Zhang, W.; Xu, H.; Guo, Q.-Y.; Liu, Y.; Luo, J.; Liu, X.-Y.; Zhang, R.; Huang, J.; Liu, T.; Su, Z.; Zhang, R.; Zhang, S.; Liu, T.; Cheng, S. Z. D. Magnifying the Structural Components of Biomembranes: A Prototype for the Study of the Self-Assembly of Giant Lipids. *Angew. Chem., Int. Ed.* **2020**, *59* (13), 5226−5234.
(31) Luo, J.; Liu, T.; Qian, K.; Wei, B.; Hu, Y.; Gao, M.; Sun, X.; Lin, Z.; Chen, J.; Bera, M. K.; Chen, Y.; Zhang, R.; Mao, J.; Wesdemiotis, C.; Tsige, M.; Cheng, S. Z. D.; Liu, T. Continuous Curvature Change into Controllable and Responsive Onion-like Vesicles by Rigid Sphere−Rod Amphiphiles. *ACS Nano* **2020**, *14* (2), 1811−1822.
(32) Zhou, Y.; Luo, J.; Liu, T.; Wen, T.; Williams-Pavlantos, K.; Wesdemiotis, C.; Cheng, S. Z. D.; Liu, T. Molecular Geometry-Directed Self-Recognition in the Self-Assembly of Giant Amphiphiles. *Macromol. Rapid Commun.* **2023**, *44* (1), 2200216.
(33) Zhu, Y.; Huang, C.; Zhang, L.; Andelman, D.; Man, X. The Process-Directed Self-Assembly of Block Copolymer Particles. *Macromol. Rapid Commun.* **2023**, *44* (17), 2300176.
(34) Huang, C.; Bai, K.; Zhu, Y.; Andelman, D.; Man, X. Design and Fabrication of Nano-Particles with Customized Properties using Self-Assembly of Block-Copolymers. *Adv. Funct. Mater.* **2024**, 2408311.
(35) Wang, Z.; Li, X.; Feng, F.; Hong, C.; Sun, Z.; Tian, W.; Yu, K.; Liu, H. Dynamic co-assembly behaviors of polyoxometalates and giant surfactants in dual solvents. *Giant* **2023**, *13*, 100142.
(36) Xia, Z.; Yang, Y.; Song, Y.-F.; Shi, S. Self-Assembly of Polyoxometalate-Based Nanoparticle Surfactants in Solutions. *ACS Macro Lett.* **2024**, *13* (2), 99−104.
(37) van der Tol, J. J. B.; Vantomme, G.; Meijer, E. W. Solvent-Induced Pathway Complexity of Supramolecular Polymerization Unveiled Using the Hansen Solubility Parameters. *J. Am. Chem. Soc.* **2023**, *145* (32), 17987−17994.
(38) Vandenburg, H. J.; Clifford, A. A.; Bartle, K. D.; Zhu, S. A.; Carroll, J.; Newton, I. D.; Garden, L. M. Factors Affecting High-Pressure Solvent Extraction (Accelerated Solvent Extraction) of Additives from Polymers. *Anal. Chem.* **1998**, *70* (9), 1943−1948.
(39) Lazzaroni, M. J.; Bush, D.; Eckert, C. A.; Frank, T. C.; Gupta, S.; Olson, J. D. Revision of MOSCED Parameters and Extension to Solid Solubility Calculations. *Ind. Eng. Chem. Res.* **2005**, *44* (11), 4075−4083.
(40) Critchfield, F. E.; Gibson Jr, J. A.; Hall, J. L. Dielectric constant and refractive index from 20 to 35° and density at 25° for the system tetrahydrofuran—Water1. *J. Am. Chem. Soc.* **1953**, *75* (23), 6044−6045.
(41) Malmberg, C.; Maryott, A. Dielectric constant of water from 0 to 100 C. *J. Res. Natl. Bur. Stand.* **1956**, *56* (1), 1−8.
(42) Provencher, S. W. CONTIN: A general purpose constrained regularization program for inverting noisy linear algebraic and integral equations. *Comput. Phys. Commun.* **1982**, *27* (3), 229−242.
(43) Hiemenz, P. C.; Rajagopalan, R. *Principles of Colloid and Surface Chemistry, Revised and Expanded*, CRC press, 2016.

https://doi.org/10.1021/acsami.4c10543
ACS Appl. Mater. Interfaces 2024, 16, 51512−51520